SUPPORTING MATERIAL
Molecular mapping of general anesthetic sites in a voltage-gated ion channel

Annika F. Barber, Qiansheng Liang, Cristiano Amaral, Werner Treptow &
Manuel Covarrubias

MATERIALS AND METHODS

Molecular biology and site-directed mutagenesis

The K-Shaw2-F335A was used as the "wild-type" background. This mutant is advantageous because it expresses currents that are much larger than the true wild-type and exhibits only slightly enhanced sensitivity to n-alcohols. All cDNAs encoding the investigated Kv channels were maintained as previously reported (4) and site-directed mutagenesis (Ala/Val scanning) was conducted according to the QuickChange protocol (Stratagene, La Jolla, CA). When a position was occupied by Ala in the wild-type K-Shaw2, the residue was mutated to Val; and, in some instances, Thr was mutated to Val, when the Ala mutation failed to express. All mutations were verified by automated DNA sequencing (Kimmel Cancer Center, Thomas Jefferson University).

Reagents

Immediately before the experiments, HPLC grade 1-BuOH (Fisher Scientific, Hampton, NH) and halothane (Halocarbon Laboratories, River Edge, NJ) were diluted to the desired final concentrations. As previously described, halothane was prepared and diluted using gastight methods to prevent loss of the volatile compound (2). Halothane concentrations in solutions and perfusates were determined by HPLC. The loss of halothane in our system was <5%. Halothane is stabilized by addition of 0.1% thymol, which did not affect K-Shaw2 currents at concentrations as high as 1 mM.

Heterologous expression

Care and surgery of *Xenopus laevis* frogs was performed according to a protocol approved by the Thomas Jefferson University IACUC. As described previously (4, 8, 9), the heterologous expression of wild-type and mutant K-Shaw2 channels in *Xenopus o*ocytes was achieved by microinjection of in vitro transcribed mRNA (mMessage mMachine kit, Ambion, Austin, TX). Typically, currents were investigated 12-48 h post-microinjection. K-Shaw2-F335A begins to express 6-12 h post-microinjection.

Electrophysiology

Whole-oocyte currents were recorded at room temperature (21-23°C) under two-electrode voltage-clamp conditions. Data acquisition, leak subtraction and initial analysis were performed using pClamp 9.2 (Molecular Devices, Sunnyvale, CA). Macroscopic currents were low-pass filtered at 0.5-1 kHz and digitized at 1-2 kHz. Leak current was subtracted offline assuming a linear leak over the voltage range investigated.

As reported previously, a gravity-driven perfusion system with syringes containing various doses of 1-BuOH was used to deliver the anesthetic into the recording chamber (1, 2, 8, 9). The valve system was controlled manually to sequentially expose a single oocyte to various doses of the

anesthetic (Fig. 2). To test the anesthetics, the currents were evoked at intervals of 4.6 s by 400-ms depolarizations to +60mV from a holding potential of -100 mV. Only after establishing a reproducible and stable current response during the perfusion of bath solution, the oocyte in the recording chamber was exposed to the anesthetic; and, to ensure equilibrium, the next dose was delivered only after a new baseline was established. After all doses were applied, the chamber was washed out with control bath solution to test the reversibility of the cumulative response. Identical results were observed when the application of each dose was followed by a washout period. To construct the halothane dose-response curve, the plunger of a single Hamilton gas-tight syringe containing a dose of the anesthetic was controlled manually. It was therefore not possible to apply multiple doses of halothane to the same oocytes. Consequently, in all instances, each dose was measured with multiple oocytes. Then, the results from different doses were combined to construct the dose-response curve, which was characterized as described below.

Data analysis

Curve fitting and statistics. Data analysis, curve fitting, plotting and statistical testing were performed in Origin 8.0 (OriginLab, Northampton, MA). Unless otherwise indicated, all results are reported as mean ± SEM; and one-way ANOVA was used to evaluate statistical significances of apparent differences. Table S1 provides a summary of symbols used in the manuscript.

Table S1: Summary of Symbols

Symbol	Definition
$K_{0.5}$	Concentration of drug that causes 50% inhibition (i.e., IC_{50})
n_H	Hill coefficient (cooperativity index)
K	Aggregate equilibrium dissociation constant = $K_{0.5}^{n_H}$
ÄG	Apparent free energy change = $n_H RT \ln K_{0.5}$
ÄÄG	The energetic impact of the mutations = ÄG_{MUT} – ÄG_{WT}
Ù	The coupling coefficient = $(K_{WT} \times K_{DM}) / (K_{M1} \times K_{M2})$. If the energetic effect of the combined mutations is additive (not coupled), Ù=1.
E_Ω	Coupling energy = $RT \ln(Ù)$
B_i	Effective molecular binding constant from AutoDock calculations for each binding site (i) (See Supporting Material pages 5-6)

$K_{0.5}$, n_H, K, ÄG and ÄÄG were each independently calculated for individual oocytes and errors were determined for averages of these independent values. Standard error for Ù and E_Ω were calculated assuming linear propagation.

Dose-response curves and energetics. Dose-response curves were characterized as previously described (2). Briefly, normalized dose-inhibition curves were empirically described by assuming this form of the Hill equation:

$$\frac{I}{I_0} = \frac{1}{1 + (\frac{x}{K_{0.5}})^{n_H}}$$

where I is the inhibited current, I_0 is the control current and x is the anesthetic concentration. The best-fit to this equation returned the $K_{0.5}$ and n_H (Table S1). The aggregate equilibrium dissociation constant was calculated as $K = K_{0.5}^{n_H}$, all calculations were performed with molar units.

The apparent free energy change was calculated as $\Delta G = n_H RT \ln K_{0.5}$, and the energetic impact of the mutations ($\Delta\Delta G$) was calculated as $\Delta\Delta G = \Delta G_{MUT} - \Delta G_{WT}$. The standard error for $\Delta\Delta G$ was propagated according to the equation:

$$\alpha_{\Delta\Delta G} = \sqrt{\alpha^2_{\Delta G_{WT}} + \alpha^2_{\Delta G_{Mut}}}$$

Hill equation fitting was performed for each individual oocyte in response to 1-BuOH, yielding independent measurements of $K_{0.5}$, n_H, aggregate K, ÄG and ÄÄG for each oocyte.

Double mutant cycle analysis (DMCA) was conducted to assess the additivity of free energy changes according to the scheme depicted below (3, 11, 23, 24).

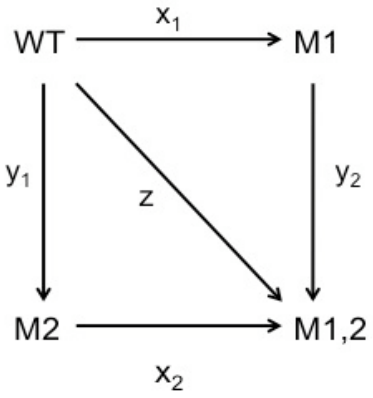

Here, $\frac{x_1}{x_2} = \frac{y_1}{y_2}$, which in terms of the measured parameters (aggregate K) defines the coupling coefficient Ω as

$$\Omega = \frac{K_{WT} \times K_{DM}}{K_{M1} \times K_{M2}}$$

Thus, if the energetic effect of the mutations is additive, Ω=1. The standard error of Ω (α_Ω) was calculated assuming linear error propagation according to the following equation:

$$\alpha_\Omega = \Omega \sqrt{\left(\frac{\alpha_{Dbl}}{K_{Dbl}}\right)^2 + \left(\frac{\alpha_{WT}}{K_{WT}}\right)^2 + \left(\frac{\alpha_{Mut1}}{K_{Mut1}}\right)^2 + \left(\frac{\alpha_{Mut2}}{K_{Mut2}}\right)^2}$$

Then, the coupling energy (E_Ω) was calculated as $RT\ln(\Omega)$, and the corresponding errors were propagated as:

$$\alpha(E_\Omega) = RT\,\frac{\alpha_\Omega}{\Omega}$$

Estimation of gating parameters. To characterize possible effects on channel gating, three empirical parameters were estimated for each mutant. The degree of inactivation was determined by evaluating I_{peak}/I_{400ms} for each current record at +70 mV; where I_{peak} is the peak current and I_{400m}s is the current amplitude at t = 400 ms of the depolarizing step. Changes in the rate of activation were determined by calculating the $T_{0.5}$ at +70 mV for each current record, the time at which the current reached half-maximum. In some cases, however, activation was nearly instantaneous. K-Shaw2 has a very low open probability (P_o) and weak voltage dependence. Consequently, maximum P_o cannot be attained within an achievable voltage range in oocytes (19, 20). This limitation prohibits construction of traditional conductance-voltage (G-V) curves and accurate estimation of the best-fit Boltzmann function to derive the activation parameters ($V_{1/2}$ and z, midpoint voltage and equivalent gating charge, respectively). Thus, in lieu of changes in activation $V_{1/2}$, an empirical ΔV was obtained from normalized current-voltage plots to characterize shifts in voltage dependence. ΔV was calculated by determining the maximum x-axis difference between normalized mutant and wild-type curves (Fig. S2B).

Building the K-Shaw2 homology model

Based on the published X-ray crystal structure (14), we modeled the membrane-bound structure of Kv1.2 in the open (activated) and closed (resting) states. Modeling details and validation of the Kv1.2 atomistic structures that satisfy experimental distance constraints were reported previously (6, 21). Given a sequence similarity of ~80% between Kv1.2 and K-Shaw2, a complete atomistic homology model of K-Shaw2 in the closed and open states was built based on the membrane equilibrated structures of Kv1.2. The primary sequence of K-Shaw2 was taken from the Swiss-Prot, entry number P17972. Then, the Modeller software (http://salilab.org/modeller/) was used to generate the K-Shaw2 atomistic models.

The macromolecular system (channel + membrane) for each of the starting K-Shaw2 models was built up as follows. Each of the starting K-Shaw2 structures possessed five well-defined cavities. One central cavity located below the selectivity filter and four cavities located in the voltage-sensor domains. As the latter may correspond to hydrated regions of the protein with direct implications in the function of the channel, each protein model was fully hydrated before placing it in a membrane model. The channel constructs were then inserted at the center of a membrane patch composed by palmitoyl-oleyl-phosphatidylcholine (POPC) lipid molecules, optimizing the distance between conserved aromatic side chains (belonging to S1 through S3) and the phospholipid head groups. The complete systems contain the K-Shaw2 channel, 390 lipid molecules, 26280 solvent-water molecules and 2 potassium ions located in the selectivity filter (a total of 122,988 atoms). To ensure the neutrality of the system, 14 counter ions (chloride) were distributed uniformly in the solvent. The initial dimensions of the simulation cell were 124.672 x 126.874 x 89.8839 $Å^3$.

Molecular dynamics

The MD simulations were carried out in the NPT ensemble using the program NAMD2 (18) and periodic-boundary conditions (PBC). The equations of motion were integrated using a multiple time-step algorithm (12). Short- and long-range forces were calculated every 1 and 2 time-steps respectively, with a time step of 2.0 fs. Langevin dynamics and Langevin piston methods were applied to keep the temperature (300 K) and the pressure (1 atm) of the system fixed. Chemical bonds between hydrogen and heavy atoms were constrained to their equilibrium value. Long-range electrostatic forces were taken into account using the particle mesh Ewald (PME) approach (5). The water molecules were described using the TIP3P model (13). The simulation used the CHARMM22-CMAP force field with torsional cross-terms for the protein (15, 16) and CHARMM27 for the phospholipids (7). A united-atom representation was adopted for the acyl chains of the POPC lipid molecules (10).

For each K-Shaw2 simulation, the channel was initially relaxed embedded in the membrane for ~4.0 ns with the protein coordinates constrained harmonically around the starting structure. Constraints were applied only to backbone atoms within the secondary structure elements. This procedure ensured a uniform and tight distribution of lipid molecules around the protein without disturbing the initial conformation. The harmonic constraints were then released for multi-ns relaxation of the full channel system by means of unconstrained MD simulation spanning ~15 ns. Execution of NAMD2 was performed on 12 Quad Core Intel 64-bit Xeon E5410 processors (2.33 GHz) of a local cluster.

Docking calculations

1-BuOH and halothane were docked separately on K-Shaw2 (closed), K-Shaw2 (open) and Kv1.2 (closed). Given that the channel conformational flexibility influences ligand binding, the anesthetics were docked against a family of ten equilibrium conformations for each of the channel structures. The conformations for K-Shaw2 in the open and closed sates were sampled throughout the last 5 ns of the corresponding equilibrium MD simulations. The MD simulations providing the Kv1.2 conformations were described elsewhere (6).

Using the program AutoDock 4.2 (17), a total of 30 independent docking calculations were performed for each ligand. Each docking calculation consisted of two hundred and fifty runs of Lamarckian genetic algorithm (LGA), with initial population size of 600 individuals. The ligand was docked on the receptor structure by considering a grid of 126 x 126 x 80 $Å^3$, with 0.45 Å spacing and containing the intracellular portions of the channel segments S5, S6 and the S4-S5 linker. Chemical bonds in the ligand were flexible. By considering a RMS tolerance of 0.5 Å, we recovered respectively a total of 1412, 1465 and 1511 docking solutions for 1-BuOH on K-Shaw2 (closed), K-Shaw2 (open) and Kv1.2 (closed), respectively. The total number of docking solutions recovered for halothane on the respective structures was 394, 477 and 353.

The docking solutions were clustered into sites according to their specific location on the channel structure. The affinity of the ligand for a binding site i was then computed by defining the ligand binding constant, B_i:

$$B_i = \frac{\sum_{j=1}^{N} E_j \delta_{ij}}{Z}$$

where, E_j is the energy of the docking solution j and $Z = \sum_{j=1}^{N} E_j$ is the cumulative energy over the total number N of docking solutions. Here, $\delta_{ij} = 1$ for every j matching i and $\delta_{ij} = 0$ otherwise. The binding energy E, as provided by Autodock, includes van der Waals, hydrogen bond and electrostatic terms for the ligand-protein interactions, as well as the ligand torsion and implicit solvation.

REFERENCES

1. Bhattacharji, A., B. Kaplan, T. Harris, X. Qu, M. W. Germann, and M. Covarrubias. 2006. The concerted contribution of the S4-S5 linker and the S6 segment to the modulation of a Kv channel by 1-alkanols. Mol. Pharmacol. 70: 1542-1554 PM:16887933.

2. Bhattacharji, A., N. Klett, R. C. Go, and M. Covarrubias. 2010. Inhalational anaesthetics and n-alcohols share a site of action in the neuronal Shaw2 Kv channel. Br. J. Pharmacol. 159: 1475-1485 PM:20136839.

3. Carter, P. J., G. Winter, A. J. Wilkinson, and A. R. Fersht. 1984. The use of double mutants to detect structural changes in the active site of the tyrosyl-tRNA synthetase (Bacillus stearothermophilus). Cell 38: 835-840 PM:6488318.

4. Covarrubias, M., T. B. Vyas, L. Escobar, and A. Wei. 1995. Alcohols inhibit a cloned potassium channel at a discrete saturable site. Insights into the molecular basis of general anesthesia. J. Biol. Chem. 270: 19408-19416.

5. Darden, T., D. York, and L. Pedersen. 1993. Particle mesh Ewald - An Nlog(N) method for Ewald sums in large systems. J. Chem. Phys. 98: 10089-10092.

6. Delemotte, L., W. Treptow, M. L. Klein, and M. Tarek. 2010. Effect of sensor domain mutations on the properties of voltage-gated ion channels: molecular dynamics studies of the potassium channel Kv1.2. Biophys. J. 99: L72-L74 PM:21044565.

7. Feller, S. E., and A. D. Mackerell Jr. 2000. An improved empirical potential energy function for molecular simulations of phospholipids. J. Phys. Chem. B 104: 7510-7515.

8. Harris, T., A. R. Graber, and M. Covarrubias. 2003. Allosteric modulation of a neuronal K^+ channel by 1-alkanols is linked to a key residue in the activation gate. Am. J. Physiol Cell Physiol 285: C788-C796 PM:12958027.

9. Harris, T., M. Shahidullah, J. S. Ellingson, and M. Covarrubias. 2000. General anesthetic action at an internal protein site involving the S4-S5 cytoplasmic loop of a neuronal K^+ channel. J Biol. Chem. 275: 4928-4936 PM:10671530.

10. Henin, J., W. Shinoda, and M. L. Klein. 2008. United-atom acyl chains for CHARMM phospholipids. J. Phys. Chem. B 112: 7008-7015 PM:18481889.

11. Hidalgo, P., and R. MacKinnon. 1995. Revealing the architecture of a K^+ channel pore through mutant cycles with a peptide inhibitor. Science 268: 307-310 PM:7716527.

12. Izaguirre, J. A., S. Reich, and R. D. Skeel. 1999. Longer time steps for molecular dynamics. J. Chem. Phys. 110: 9853-9864.

13. Jorgensen, W. L., J. Chandrasekhar, J. D. Madura, R. W. Impey, and M. L. Klein. 1983. Comparison of simple potential functions for simulating liquid water. J. Chem. Phys. 79: 926-935.

14. Long, S. B., E. B. Campbell, and R. MacKinnon. 2005. Voltage Sensor of Kv1.2: Structural Basis of Electromechanical Coupling. Science 309: 903-908 PM:16002579.

15. Mackerell Jr., A. D., D. Bashford, M. Bellot, R. L. Dunbrack Jr., J. D. Evanseck, and et al. 1998. All-atom empirical potential for molecular modeling and dynamics studies of proteins. J. Phys. Chem. B B 102: 3586-3616.

16. Mackerell, A. D., Jr., M. Feig, and C. L. Brooks, III. 2004. Improved treatment of the protein backbone in empirical force fields. J. Am. Chem. Soc. 126: 698-699 PM:14733527.

17. Morris, G. M., R. Huey, W. Lindstrom, M. F. Sanner, R. K. Belew, D. S. Goodsell, and A. J. Olson. 2009. AutoDock4 and AutoDockTools4: Automated docking with selective receptor flexibility. J. Comput. Chem. 30: 2785-2791 PM:19399780.

18. Phillips, J. C., R. Braun, W. Wang, J. Gumbart, E. Tajkhorshid, E. Villa, C. Chipot, R. D. Skeel, L. Kale, and K. Schulten. 2005. Scalable molecular dynamics with NAMD. J. Comput. Chem. 26: 1781-1802 PM:16222654.

19. Smith-Maxwell, C. J., J. L. Ledwell, and R. W. Aldrich. 1998. Role of the S4 in cooperativity of voltage-dependent potassium channel activation. J. Gen. Physiol. 111: 399-420.

20. Smith-Maxwell, C. J., J. L. Ledwell, and R. W. Aldrich. 1998. Uncharged S4 residues and cooperativity in voltage-dependent potassium channel activation. J. Gen. Physiol. 111: 421-439.

21. Treptow, W., and M. Tarek. 2006. Environment of the gating charges in the Kv1.2 Shaker potassium channel. Biophys. J. 90: L64-L66 PM:16533847.

22. Treptow, W., and M. Tarek. 2006. K+ conduction in the selectivity filter of potassium channels is monitored by the charge distribution along their sequence. Biophys. J. 91: L81-L83 PM:16980355.

23. Wells, J. A. 1990. Additivity of mutational effects in proteins. Biochemistry 29: 8509-8517 PM:2271534.

24. Yifrach, O., and R. MacKinnon. 2002. Energetics of pore opening in a voltage-gated K^+ channel. Cell 111: 231-239 PM:12408867.

SUPPORTING FIGURES

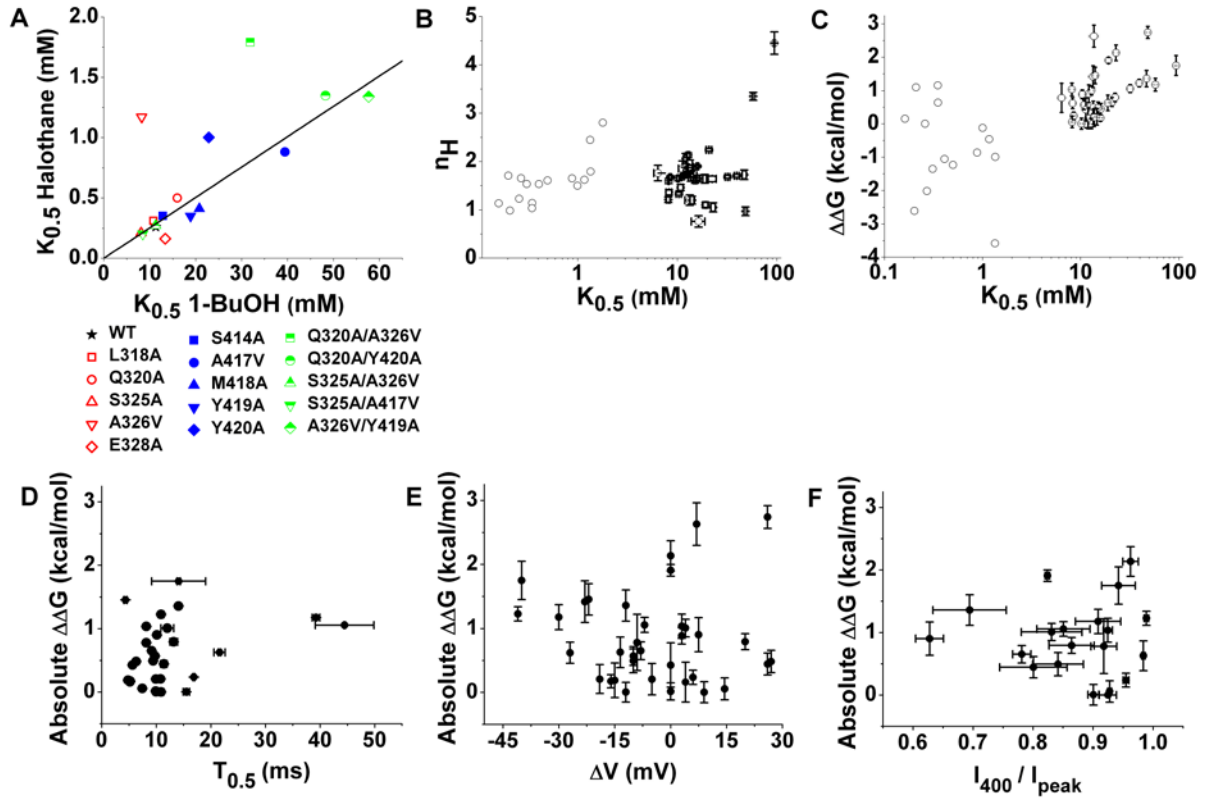

FIGURE S1. Correlations between Hill equation parameters, $\Delta\Delta G$ and gating parameters. *(A)* Correlation of the $K_{0.5}$ values for 1-BuOH and halothane. The line represents the best fit linear regression ($R^2 = 0.95$). Wild-type indicated with a black star, S4-S5 residues indicated in red, S6 in blue and double mutants in green. Two apparent outliers were excluded from the regression analysis. *(B)* Semi-log scatter plot of $K_{0.5}$ vs. n_H for all mutants. Halothane data is shown without error bars. These parameters are not correlated whether drugs are considered separately or together. (R^2 from linear fit to all data= 0.07). *(C)* Semi-log scatter plot of $\Delta\Delta G$ vs. $K_{0.5}$. Halothane data is shown without error bars. These parameters are not correlated whether drugs are considered separately or together (R^2 from linear fit to all data = 0.26). *(D)* Scatter plot of $\Delta\Delta G$ vs. $T_{0.5}$. The $T_{0.5}$ was measured as explained under Materials and Methods. *(E)* Scatter plot of $\Delta\Delta G$ vs. ΔV. The maximal shift in the normalized current-voltage plot (ΔV) was calculated as explained under Materials and Methods. *(F)* Scatter plot of vs. I_{400}/I_{peak}. This ratio measures the degree of current inactivation at 400 ms. Note that there is no apparent correlation between $\Delta\Delta G$ and the three empirical gating parameters.

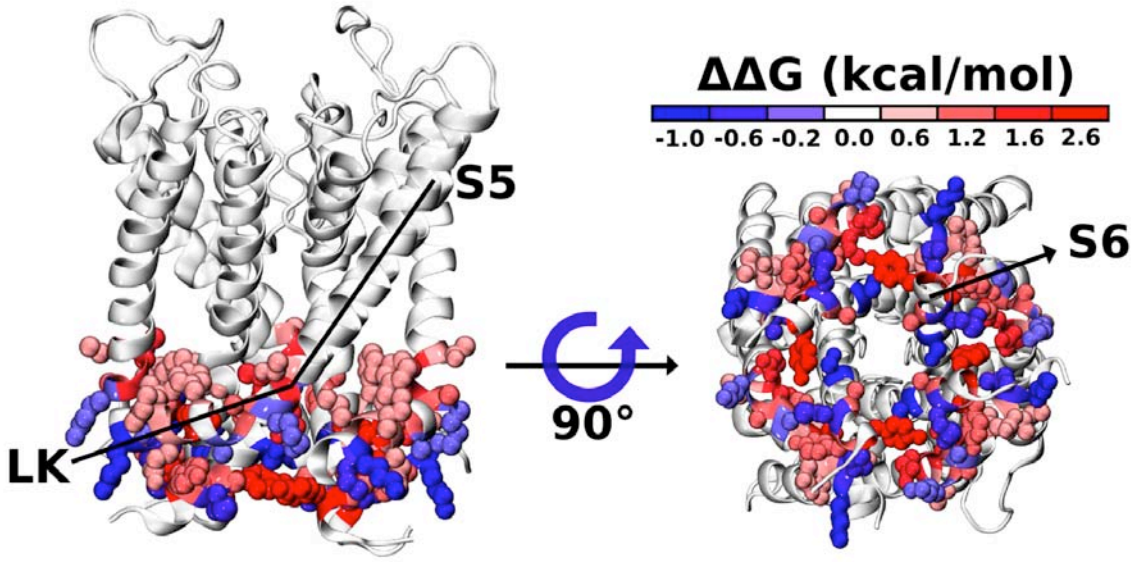

FIGURE S2 Thermodynamic molecular map of free energy changes induced by mutations in the S4-S5 linker and S6 segment of K-Shaw2. Lateral *(left)* and bottom *(right)* views of the K-Shaw2 closed structure showing the energetic impact of single mutations ($\Delta\Delta G$) on the channel inhibition by 1-BuOH. For clarity, only the channel S4-S5 linker (LK) and the pore segments S5 through S6 are depicted and only mutated residues are shown in space-filling view. Residues whose mutation yielded a positive $\Delta\Delta G$ for 1-BuOH (less favorable impact) are shown in red, while residues whose mutation yielded a negative $\Delta\Delta G$ (more favorable impact) are shown in blue.

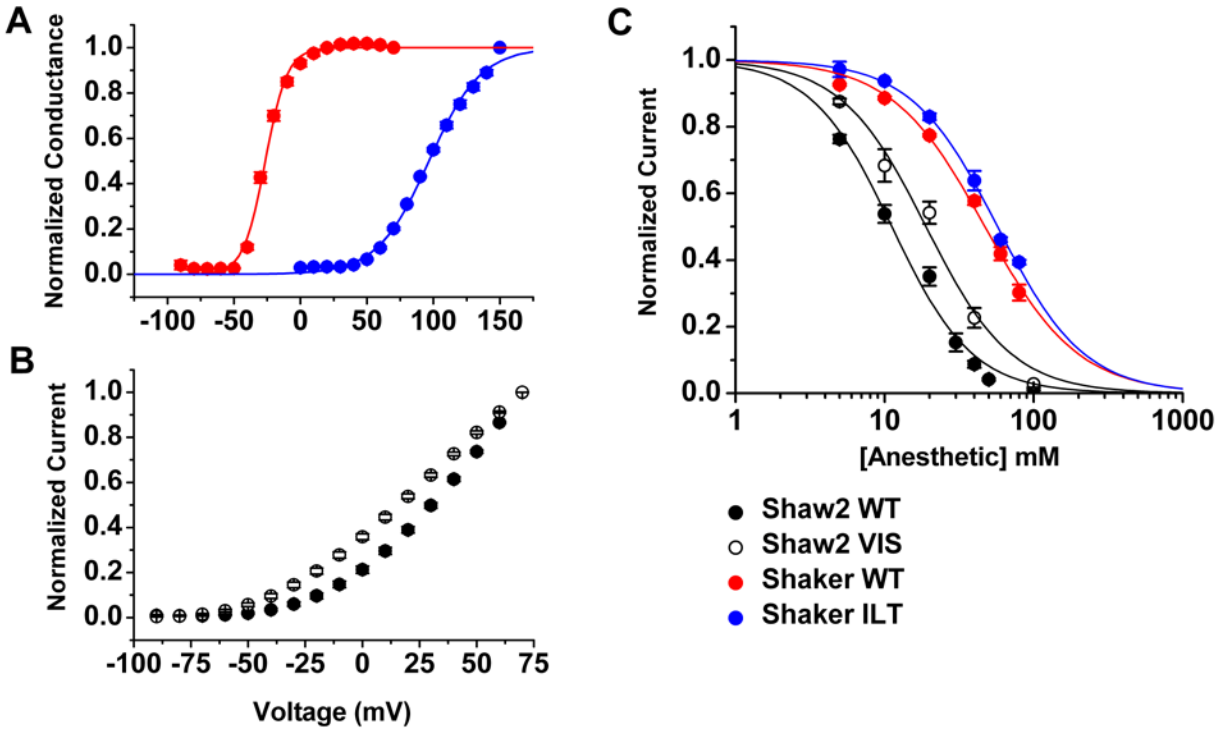

FIGURE S3. 1-BuOH sensitivity of Kv channels with distinct voltage dependencies. *(A)* The voltage sensor ShakerB-ILT mutant exhibits a large depolarizing shift ($V_{1/2}$ = +97 mV, slope factor = 20 mV) compared to WT ($V_{1/2}$ = -26 mV, slope factor = 8 mV). *(B)* The reverse VIS triple mutation in K-Shaw2 causes only a mild leftward shift (ΔV = -20mV). *(C)* The ShakerB-ILT mutant retained the characteristic 1-BuOH insensitivity of wild-type ShakerB. The ShakerB-ILT dose response was constructed at +100 mV, the ShakerB WT dose response was constructed at +60 mV. The lines are the best fits to the Hill equation (ILT: $K_{0.5}$=57 mM, n_H=1.5; wild-type: $K_{0.5}$=47 mM, n_H=1.4). The K-Shaw2-VIS mutation decreased 1-BuOH sensitivity modestly (VIS: $K_{0.5}$=19 mM, n_H=1.5; wild-type: $K_{0.5}$=11 mM, n_H=1.6). Both K-Shaw2 dose-response curves were constructed at +60 mV as described under Materials and Methods above.

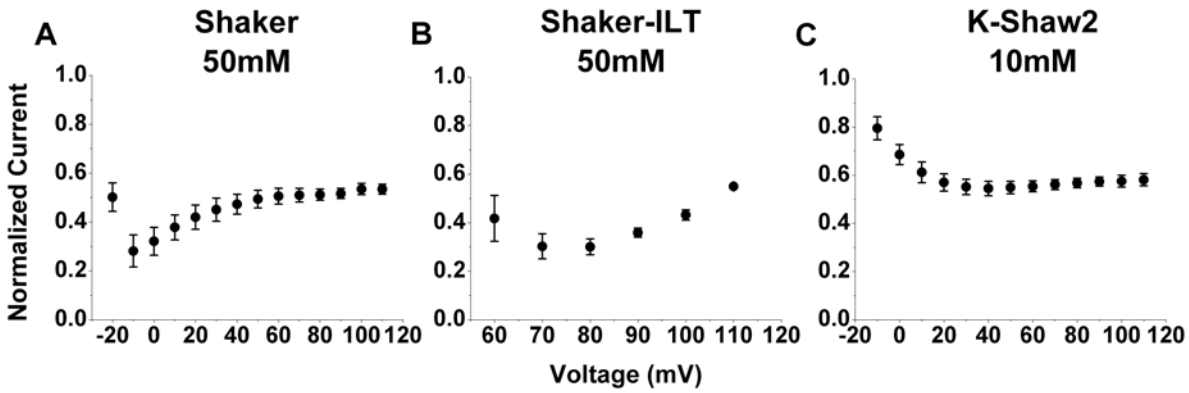

FIGURE S4. Voltage dependence of 1-BuOH action. *(A)* A voltage step protocol was applied to ShakerB expressed in *Xenopus* oocytes in the presence and absence of 50 mM 1-BuOH. The current in the presence of drug was then divided by the baseline (drug-free) current to yield a normalized current at each voltage. Only voltages at which the current was observed are shown. *(B)* Voltage dependence of Shaker-ILT mutant, calculated as in panel A. *(C)* Voltage dependence of K-Shaw2, calculated as in panel A with 10 mM 1-BuOH. Note that the trend is preserved in all panels. At very low Po, channels are somewhat resistant to inhibition. Inhibition then reaches some trough at a voltage and then climbs again (albeit gradually in C).

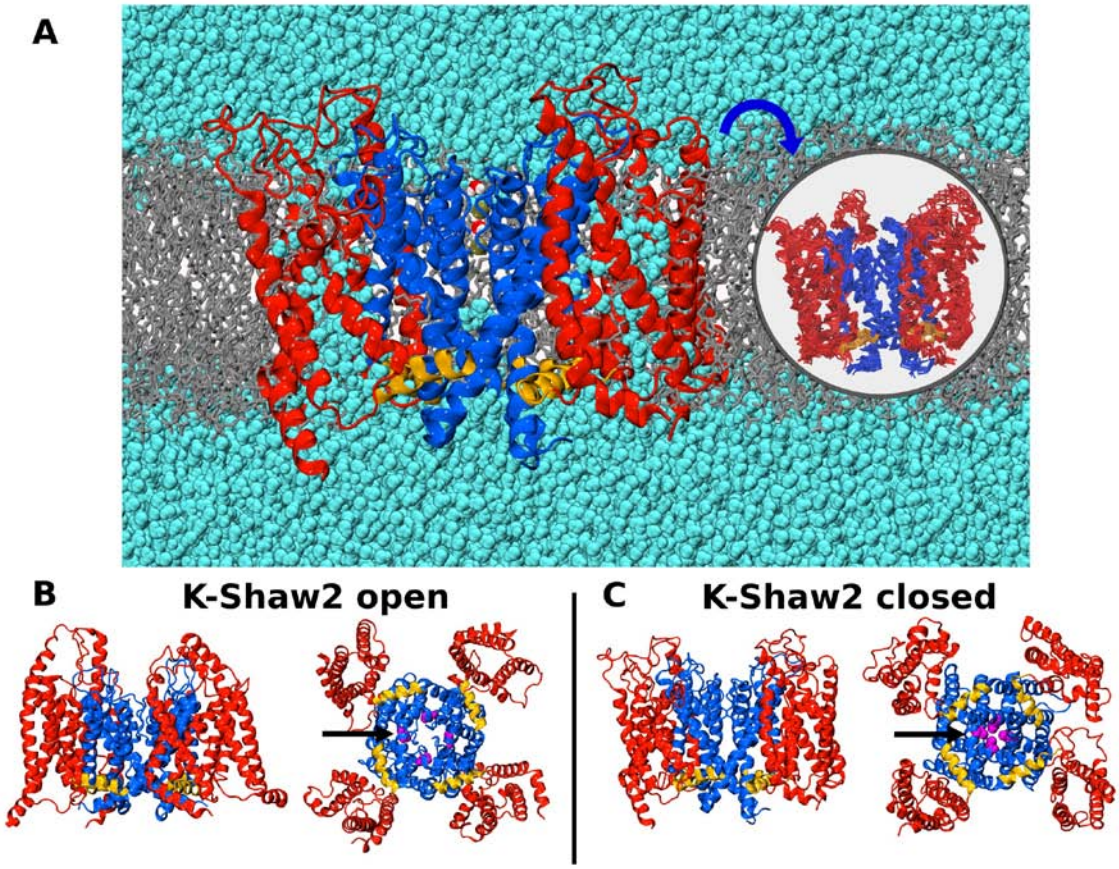

FIGURE S5. MD simulation of the K-Shaw2 channel. *(A)* Simulation system containing the K-Shaw2 channel (red: voltage sensor; orange: S4-S5 linker; blue: pore) embedded in a fully-hydrated patch of POPC lipid bilayer (gray). Two K^+ ions (ochre) and two water molecules are shown at the selectivity filter. Inset shows overlay of ten equilibrium structures to highlight backbone flexibility. *(B* and *C)* Membrane-equilibrated structures of K-Shaw2 in the open and closed states. Note that V409 (pink) forms a hydrophobic gate that controls ion conduction, as previously reported for other Kv channels (22).

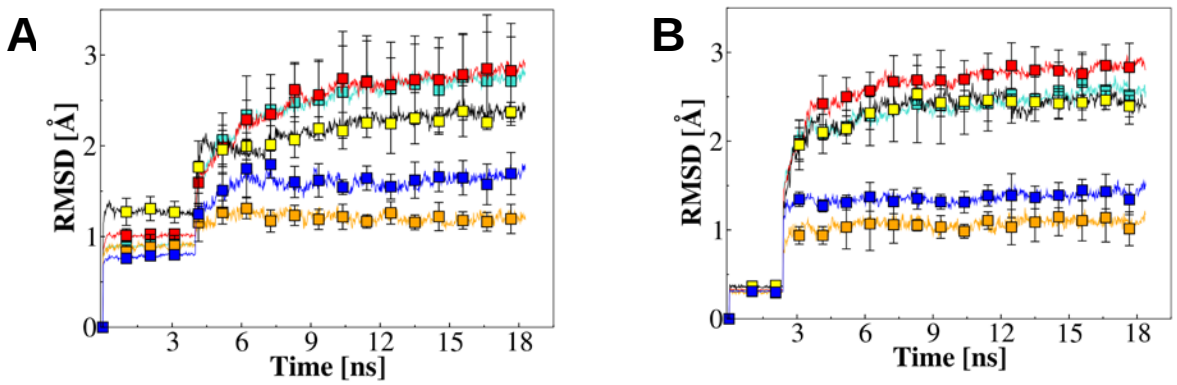

FIGURE S6. RMSD profiles for the K-Shaw2 MD simulation. Root-mean-square deviation (rmsd) profiles for the simulation of K-Shaw2 closed *(A)* and *(B)* open conformations. Profiles for the channel's fragments, i.e voltage sensor (red), S4 (yellow), S4-S5 linker (orange), pore (blue) and the TM domain (cyan) are depicted. The Shaw2 structure was constrained during the equilibration stage to allow for full reorganization of the water and lipids. The rmsd values were calculated with respect to the initial atomistic structure by superposing the main-chain atoms.

FIGURE S7. 1-BuOH docking calculations. The K-Shaw2 channel (open and closed) exhibits a total of eight possible docking sites. The colored density blobs indicate the location of the sites in the lateral *(A)* and bottom *(B)* views, which are compared against Kv1.2. *(C)*. Binding constants were estimated in Autodock. See Materials and Methods and Figure 6 legend for more details.

Table S2: Parameters of the interaction of 1-BuOH with K-Shaw2

Mutant	N	$K_{0.5}$ mM	n_H	Aggregate *K* mM	Ä*G* kcal/mol	ÄÄ*G* kcal/mol	Coupling energy kcal/mol
WT (F335A)	29	11.33 ± 0.50	1.69 ± 0.31	0.61 ± .08	-4.53 ± 0.09	0	
S4-S5 LINKER							
K316A	10	12.09 ± 0.54	2.06 ± 0.10*	0.46 ± 0.15	-4.90 ± 0.25	-0.90 ± 0.27	
I317A	8	13.42 ± 0.78	1.95 ± 0.08*	0.29 ± 0.08	-4.98 ± 0.17	-0.49 ± 0.07	
L318A	7	10.81 ± 0.63	1.46 ± 0.06*	1.56 ± 0.32	-3.90 ± 0.12	-0.57 ± 0.15	
I319A	8	12.75 ± 0.66	1.73 ± 0.04	0.59 ± 0.09	-4.46 ± 0.10	0.01 ± 0.13	
Q320A	7	16.02 ± 0.07*	1.65 ± 0.06	1.32 ± 0.33	-4.04 ± 0.15	0.44 ± 0.17	
T321V	3	13.64 ± 1.50*	1.15 ± 0.14*	13.51 ± 6.48	-2.98 ± 0.41	1.50 ± 0.43	
F322A	5	14.65 ± 1.06*	1.71 ± 0.11	0.93 ± 0.28	-4.28 ± 0.23	0.21 ± 0.25	
R323A	7	12.84 ± 0.41	1.74 ± 0.05	0.58 ± 0.12	-4.49 ± 0.13	-0.004 ± 0.15	
A324V	6	13.47 ± 0.63	1.84 ± 0.09	0.48 ± 0.13	-4.68 ± 0.21	-0.21 ± 0.23	
S325A	12	8.13 ± 0.33*	1.21 ± 0.06*	4.90 ± 1.34	-3.40 ± 0.16	1.04 ± 0.19	
A326V	11	8.26 ± 0.56*	1.36 ± 0.05*	1.89 ± 0.43	-3.88 ± 0.14	0.62 ± .17	
K327A	5	11.89 ± 0.36	1.77 ± 0.11	0.60 ± 0.20	-4.63 ± 0.30	-0.16 ± 0.31	

E328A	4	13.37 ± 1.48	1.20 ± 0.11*	7.37 ± 2.38	-3.08 ± 0.31	1.42 ± 0.33	
L329A	5	14.07 ± 0.64*	1.20 ± 0.08*	8.03 ± 3.24	-3.04 ± 0.23	1.45 ± 0.25	
T330V	6	13.69 ±0.87	1.69 ± 0.10	0.75 ± 0.35	-4.64 ± 0.26	0.19 ± 0.27	
S6 SEGMENT							
S414A	5	12.86 ± 0.49	2.13 ± 0.05*	0.10 ± 0.02	-5.48 ± 0.12	-1.01 ± 0.14	
A417V	6	39.44 ± 2.24*	1.70 ± 0.03	4.16 ± 0.42	-3.26 ± 0.07	1.23 ± 0.11	
M418A	4	20.81 ± 1.38*	2.24 ÷ 0.03*	0.18 ± 0.03	-5.15 ± 0.12	-0.65 ± 0.14	
Y419A	6	18.87 ± 0.76*	1.64 ± 0.09	2.12 ± 0.78	-3.85 ± 0.22	0.63 ± 0.24	
Y420A	5	22.87 ± 1.13*	1.05 ± 0.09*	22.85 ± 5.50	-2.36 ± 0.22	2.13 ± 0.24	
DOUBLE MUTANTS							
L318A/K327A	4	10.19 ± 0.26	1.65 ± 0.05	0.58 ± 0.12	-4.48 ± 0.14	0.002 ± 0.16	-0.57 ± 0.27
Q320A/T321V	5	6.4 ± 0.48*	1.76 ± 0.16	0.25 ± 0.10	-5.27 ± 0.43	-0.78 ± 0.44	-3.50 ± 0.45
Q320A/A326V	6	31.91 ± 1.79*	1.68 ± 0.03	3.15 ± 0.39	-3.44 ± 0.08	1.06 ± 0.12	-0.14 ± 0.22
Q320A/T330V	9	15.07 ± 0.66*	1.61 ± 0.06	1.64 ± 0.67	-4.01 ± 0.15	0.48 ± 0.17	0.01 ± 0.40
Q320A/A417V	6	46.95 ± 2.21*	1.73 ± 0.10	4.81 ± 0.87	-3.33 ± 0.23	1.36 ± 0.24	-0.36 ± 0.20
Q320A/M418A	6	22.38 ± 2.16*	1.64 ± 0.06	2.07 ± 0.32	-3.69 ± 0.09	0.79 ± 0.13	0.99 ± 0.21
Q320A/Y420A	3	48.28 ± 1.45*	0.97 ± 0.09*	58.47 ± 15.61	-1.76 ± 0.16	2.74 ± 0.18	0.10 ± 0.26

S325A/A326V	6	11.29 ± 1.03	1.85 ± 0.16	0.40 ± 0.10	-4.89 ± 0.34	-0.43 ± 0.35	-2.11 ± 0.27
S325A/T330V	5	10.37 ± 0.63	1.33 ± 0.03*	2.43 ± 0.38	-3.59 ± 0.10	0.88 ± 0.13	-0.52 ± 0.34
S325A/A417V	5	8.50 ± 0.26*	1.67 ± 0.03	0.35 ± 0.04	-4.72 ± 0.07	-0.24 ± 0.11	-1.52 ± 0.24
A326V/A417V	5	93.87 ± 1.41*	4.45 ± 0.23*	0.04 ± 002	-6.23 ± 0.29	-1.75 ± 0.30	-2.02 ± 0.26
A326V/Y419A	4	57.66 ± 1.38*	3.35 ± 0.08*	0.08 ± 0.02	-5.67 ± 0.17	-1.18 ± 0.19	-2.91 ± 0.30
A326V/Y420A	5	19.18 ± 1.07*	1.1 ± 0.05*	12.98 ± 0.71	-2.57 ± 0.03	1.91 ± 0.09	-3.96 ± 0.21

$K_{0.5}$ and n_H are averaged from best fits to the Hill equation. See Materials and Methods for calculations of energetic parameters. All errors are standard errors and asterisks indicate $P_{ANOVA}<0.05$. All aggregate *Ks* are significantly different from wild-type. Values of $K_{0.5}$, n_H, aggregate K, ÄG and ÄÄG are averages from independent (single oocyte) measurements, consequently when errors are large these numbers cannot be used directly to calculate average values of downstream parameters.

Table S3: Parameters of the interaction of halothane with K-Shaw2

Mutant	N	$K_{0.5}$	n_H	Aggregate *K*	Ä*G*	ÄÄ*G*	Coupling Energy
		mM		mM	kcal/mol	kcal/mol	kcal/mol
WT	45	0.26	1.23	$3.93x10^{-02}$	-6.01		
S4-S5 LINKER							
L318A	13	0.31	1.54	$4.10x10^{-03}$	-7.36	-1.35	
Q320A	17	0.50	1.61	$4.92x10^{-03}$	-7.24	-1.23	
S325A	17	0.21	0.98	$2.39x10^{-01}$	-4.91	1.10	
A326V	12	1.17	1.62	$1.76x10^{-02}$	-6.47	-0.46	
E328	20	0.16	1.13	$4.96x10^{-02}$		0.15	
S6 SEGMENT							
A417V	9	0.88	1.65	$9.08x10^{-03}$	-6.87	-0.86	
M418A	9	0.41	1.53	$6.37x10^{-03}$	-7.06	-1.05	
Y419A	12	0.35	1.03	$2.69x10^{-01}$	-4.85	1.16	
Y420A	15	1.00	1.50	$3.18x10^{-02}$	-6.13	-0.12	
DOUBLE MUTANTS							
Q320A/A326V	11	1.79	2.80	$1.99x10^{-05}$	-10.48	-4.47	-2.74
Q320A/Y420A	17	1.35	1.79	$7.26x10^{-03}$	-7.00	-0.99	0.35
S325A/A326V	14	0.27	1.65	$1.26x10^{-03}$	-8.02	-2.02	-2.59
S325A/A417V	12	0.20	1.71	$4.88x10^{-04}$	-8.62	-2.61	-2.75
A326V/A417V	8				Insensitive		
A326V/Y419A	17	1.34	2.45	$9.15x10^{-05}$	-9.59	-3.58	-4.17

$K_{0.5}$ and n_H are from obtained from best fits to the Hill equation. See Materials and Methods for details of calculations.

Table S4: Effect of mutation on gating parameters.

Mutant	ÄV mV	I_p/I_{400}	$T_{0.5}$ ms	ÄÄG kcal/mol
WT (F335A)		0.92 ± 0.01	10.86 ± 0.49	
K316A	7.50	0.63 ± 0.02	10.11 ± 0.28	-0.90 ± 0.27
I317A	-10.00	0.84 ± 0.04	9.44 ± 0.20	-0.49 ± 0.07
L318A	-10.00		9.75 ± 0.39	-0.57 ± 0.15
I319A	0.00		9.88 ± 0.33	0.01 ± 0.13
Q320A	26.00	0.80 ± 0.06	11.38 ± 0.59	0.44 ± 0.17
T321V	7.00		Too Fast	1.50 ± 0.43
F322A	-5.00		9.93 ± 0.31	0.21 ± 0.25
R323A	-12.00		9.97 ± 0.42	-0.004 ± 0.15
A324V	-19.00		10.77 ± 0.23	-0.21 ± 0.23
S325A	3.00	0.92 ± 0.01	8.17 ± 0.32	1.04 ± 0.19
A326V	-27.00	0.81 ± 0.01	9.46 ± 0.32	0.62 ± .17
K327A	4.00		5.18 ± 0.25	-0.16 ± 0.31
E328A	-23.00		Too fast	1.42 ± 0.33
L329A	-22.00		4.35 ± 0.31	1.45 ± 0.25
T330V	-15.00		4.83 ± 0.31	0.19 ± 0.27
S414A	4.00	0.83 ± 0.05	12.02 ± 0.59	-1.01 ± 0.14
A417V	-41.00	0.99 ± 0.004	10.88 ± 0.47	1.23 ± 0.11
M418A	-8.00	0.78 ± 0.02	9.16 ± 0.28	-0.65 ± 0.14
Y419A	-13.50	0.98 ± 0.003	21.60 ± 1.03	0.63 ± 0.24
Y420A	0.00	0.96 ± 0.01	Too fast	2.13 ± 0.24
L318A/K327A	9.00	0.90 ± 0.01	15.51 ± 0.59	0.002 ± 0.16
Q320A/T321V	-9.00	0.92 ± 0.02	8.15 ± 0.08	-0.78 ± 0.44
Q320A/A326V	-7.00	0.85 ± 0.04	44.48 ± 5.37	1.06 ± 0.12
Q320A/T330V	27.00		6.33 ± 0.19	0.48 ± 0.17
Q320A/A417V	-12.00	0.69 ± 0.06	14.05 ± 0.30	1.36 ± 0.24
Q320A/M418A	20.00	0.86 ± 0.04	13.20 ± 0.69	0.79 ± 0.13
Q320A/Y420A	26.00		Too fast	2.74 ± 0.18
S325A/A326V	0.00		5.65 ± 0.32	-0.43 ± 0.35
S325A/T330V	3.00		Too fast	0.88 ± 0.13
S325A/A417V	6.00	0.95 ± 0.005	16.88 ± 0.21	-0.24 ± 0.11
A326V/A417V	-40.00	0.94 ± 0.28	14.09 ± 4.95	-1.75 ± 0.30
A326V/Y419A	-30.00	0.91 ± 0.04	39.24 ± 0.69	-1.18 ± 0.19
A326V/Y420A	0.00	0.82 ± 0.004	Too fast	1.91 ± 0.09

Errors are standard errors, see Methods for calculation of activation parameters.

Table S5: Residue distance from ligand isosurface

Residue	Distance
S4-S5 LINKER	**Å**
K316	11.48 ± 0.36
I317	10.10 ± 0.42
L318	4.28 ± 1.17
I319	4.90 ± 0.76
Q320	10.26 ± 0.75
T321	8.25 ± 0.31
F322	5.22 ± 0.98
R323	10.23 ± 2.54
A324	11.53 ± 1.14
S325	10.72 ± 1.24
A326	11.64 ± 2.19
K327	12.89 ± 0.42
E328	10.37 ± 0.45
L329	11.03 ± 0.99
T330	12.90 ± 1.55
S6 SEGMENT	
S414	14.45 ± 0.93
A417	16.11 ± 0.66
M418	16.07 ± 0.66
Y419	12.13 ± 0.74
Y420	14.26 ± 0.76

Distance (± standard error) is calculated between the geometrical center of protein side chains from the averaged structure and the geometrical center of the ligand cloud of docking solutions for 1-BuOH in site 3.